

Early diagenesis and carbon remineralization in young rift sediment of the Southern Okinawa Trough

Yu-Shih Lin¹, Huei-Ting Lin², Bo-Shian Wang³, Shein-Fu Wu², Pei-Ling Wang², Chih-Lin Wei², Hsiao-Fen Lee⁴, Tefang Lan⁵, Wei-Jen Huang¹, Song-Chuen Chen⁶, Yunshuen Wang⁶, and Chih-Chieh Su^{2,*}

¹Department of Oceanography, National Sun Yat-Sen University, Kaohsiung City, Taiwan

²Institute of Oceanography, National Taiwan University, Taipei City, Taiwan

³Taiwan Ocean Research Institute, National Applied Research Laboratories, Kaohsiung City, Taiwan

⁴National Center for Research on Earthquake Engineering, National Applied Research Laboratories, Taipei City, Taiwan

⁵Department of Geoscience, National Taiwan University, Taipei City, Taiwan

⁶Central Geological Survey, Ministry of Economic Affairs, New Taipei City, Taiwan

Article history:

Received 21 July 2018

Revised 12 November 2018

Accepted 10 January 2019

Keywords:

Diagenesis, Carbon remineralization, Carbon burial efficiency, Southern Okinawa Trough

Citation:

Lin, Y.-S., H.-T. Lin, B.-S. Wang, S.-F. Wu, P.-L. Wang, C.-L. Wei, H.-F. Lee, T. Lan, W.-J. Huang, S.-C. Chen, Y. Wang, and C.-C. Su, 2019: Early diagenesis and carbon remineralization in young rift sediment of the Southern Okinawa Trough. *Terr. Atmos. Ocean. Sci.*, 30, 633-647, doi: 10.3319/TAO.2019.01.10.01

ABSTRACT

With large topographic gradients, rifted basins serve as efficient traps for particulate matter from adjacent lands and the ocean surface. However, the fate of organic carbon in the sediment, mostly unaltered by the hydrothermal activities known to occur in young rifts, remains poorly understood. In this study, we present an examination of diagenetic activities and carbon remineralization based on the first complete suite of pore-water data of sediment marginally affected by hydrothermal activities in the Southern Okinawa Trough (SOT). The sediment showed an oxygen penetration depth of 1 cm, consumption of NO_3^- in the top 1 cm, smeared profiles of Mn^{2+} and Fe^{2+} with the latter reaching up to $450 \mu\text{mol L}^{-1}$, and relatively unchanged SO_4^{2-} concentrations with depth. Net production rates of dissolved species resolved from pore-water profiles provide an estimate of $1.68 \pm 0.21 \text{ mmol C m}^{-2} \text{ d}^{-1}$ as the total carbon remineralization rate in the upper 30 cm sediment column, with aerobic carbon oxidation being the major pathway. The rate, one order of magnitude lower than that of the adjacent East China Sea, is attributed to the lower bottom-water temperature and carbon flux in the trough. The high carbon burial efficiency of SOT (68% of carbon reaching the seafloor and processed thereunder) reflects the combined effects of small mountain rivers and rifting-induced particle trapping.

1. INTRODUCTION

The role of young rift systems in the global carbon cycle remains contentious. The frequently occurring coastal upwelling, in combination with the topographic gradients that facilitate material transport and burial, render rifted basins efficient traps for particulate carbon from adjacent lands and the ocean surface (e.g., Calvert 1966; Thunell et al. 1994; Sheu et al. 1999; Huh et al. 2006). On the other hand, carbon sequestration in rift sediment can be stunted by extensive magmatism and hydrothermalism (Sibuet et al. 1998; Lizarralde et al. 2011), both of which act to mo-

bilize and expel carbon back into seawater (Berndt et al. 2016; Lin et al. 2017). While the latter provides an intriguing aspect regarding how tectonism participates in carbon cycling, it should be noted that the hydrothermal activity is highly spotty at any given time (Lin et al. 2017), and carbon remineralization in the majority of young rift sediment follows early diagenesis under the baseline conditions, i.e., cold temperature with no significant advective fluid flow from deep seafloor.

The opening of the Okinawa Trough, a curved backarc basin at the convergent boundary between the Eurasian and Philippine Sea Plates, commenced during the late Miocene (9 - 6 Ma; Sibuet et al. 1998). The northbound Kuroshio Current enters the trough from the south, collides with the

* Corresponding author
E-mail: donccsu@ntu.edu.tw

shelf of the southern East China Sea (ECS), and triggers a perennial upwelling center (Liu et al. 1992; Fig. 1). Since the discovery of hydrothermal activities in the central (Sakai et al. 1990) and south sections (Konno et al. 2006) of the basin, much research effort has been devoted to the mineralogy (e.g., Glasby and Notsu 2003), biogeochemistry (e.g., De Beer et al. 2013) and microbiology (e.g., Inagaki et al. 2006) of vents and hydrothermally altered sediments, with scant attention to the baseline condition of early diagenesis. Lin et al. (2002a) first investigated the pore-water chemistry of nonhydrothermally altered sediments in the Southern Okinawa Trough (SOT). For the deep-water (> 1000 m) stations, sulfate concentrations showed a mild downward decrease of 2 - 5 mmol L⁻¹ for the top 100 cm, suggesting that redox reactions thermodynamically more favorable than sulfate reduction might prevail in this horizon. De Beer et al. (2013) reported a shallow O₂ penetration depth (< 1 cm) for their reference site sediment, alluding to the transition to O₂-depleted regimes in shallow depth. Aside from these two studies, pore-water data that can be used to infer processes other than aerobic respiration and sulfate reduction, such as concentrations of NO₃⁻, Mn²⁺, Fe²⁺, etc., are missing in the literature. Having the redox regime identified is crucial for subsequent modeling work, which usually relies on the selection of appropriate Redfield stoichiometry for reactions of organic matter remineralization (e.g., Emerson et al. 1980; Boudreau 1987).

This study attempts to portray the diagenetic activity in the near-surface sediment under baseline conditions in the SOT. We chose sites without signatures of liquid CO₂ impregnation (to be discussed later) to represent sediment with low levels of hydrothermal alteration. We estimate the contribution of different electron acceptors to carbon remineralization based on the pore-water profiles and calculation of net solute production rates. We then compare our results with published data of the ECS, and discuss factors controlling the diagenetic activity and carbon preservation within the context of regional hydrographic and depositional setting.

2. MATERIAL AND METHODS

2.1 Site Description and Expeditions

The field sites (Fig. 1; Table 1) were examined during two expeditions: OR1-1164 (25 May to 3 June 2017) and OR1-1194 (29 April to 1 May 2018) by R/V *Ocean Research I*. As the objective of the cruise OR1-1164 was to retrieve materials affected by hydrothermal activities, sampling sites were chosen broadly based on prior knowledge of subseafloor flow fields and heat flow (Chou et al. 2019; Hsu et al. 2019; this issue), and refined to specific spots based on echosounder images acquired on site. Sites P1-A and P1-T are located in the same hydrothermal patch (Patch "P1") about 10 km west of the Yonaguni Knoll IV. Towcam images revealed the presence of mineral mounds and che-

mosynthetic communities, and the temperature anomalies in the bottom water reached up to 12°C (Chou et al. 2019; this issue). Site G2 is situated at the margin of Patch "Gas Center," about 4.5 km north of Patch P1. This patch features active venting, vent clusters, and multiple mineral mounds. A detailed seafloor survey of this patch is described elsewhere (Chou et al. 2019; this issue). The ³He/⁴He ratios for the upper 40 cm sediment at Sites P1-T and G2 are 1.2 - 1.4 and 2.4 - 2.5 R_A (R_A = ³He/⁴He ratio for air), respectively (T. Lan, unpublished data). No helium isotope data are available for the sediment at Site P1-A.

2.2 Sampling

Most of the research material was retrieved during OR1-1164. The precise underwater positioning of the corers was achieved by the use of an ultra-short baseline system (Model GAPS NG, iXBlue SAS). Short sediment cores (< 40 cm) with undisturbed sediment-water interface were retrieved by a multicorer (Mega Corer, OSIL). Longer sediment cores (< 200 cm) were recovered with a gravity corer. The coordinates and water depth of the cores used in this study are listed in Table 1.

The cores were processed within 4 h after retrieval. The overlying water of the multicores was collected with a plastic syringe and then siphoned off. Pore waters were extracted from the intact whole round cores with Rhizon suction samplers (0.1 μm porous polymer, Rhizosphere Research; Seeberg-Elverfeldt et al. 2005). The depth resolution ranged from 1 - 5 cm for the multicores and 10 - 20 cm for the gravity cores. The split for total dissolved sulfide (H₂S) analysis was immediately fixed with 5% (w/v) zinc acetate solution at a volume ratio of 2:1. The subsamples for Fe²⁺ and Mn²⁺ analyses were acidified (pH < 1.8) with concentrated HCl (SEASTAR CHEMICALS). The pore-water samples were kept at 4°C [cations, anions, H₂S, dissolved inorganic carbon (DIC)] or -20°C (nutrients) until analysis.

At each site, parallel cores were dedicated for the analyses of CH₄ concentration, porosity, and bulk properties. For CH₄ analysis, cut-off plastic syringes were used to collect material from freshly exposed sediment surface, created by cutting the liner of gravity cores into short segments or during slicing of the multicores. The samples were transferred to glass vials containing 1 N NaOH solutions, sealed with thick butyl rubber stoppers, and crimp capped. For determination of porosity and total organic carbon (TOC) content, samples were also taken with plastic syringes and transferred to pre-weighed centrifuge tubes. Samples for total sulfur (TS), total iron (Fe_T), and total manganese (Mn_T) were stored in polyethylene bags. All samples were kept at 4°C until analysis.

2.3 O₂ Profiling

O₂ profiling of the water column at Sites BG, G1,

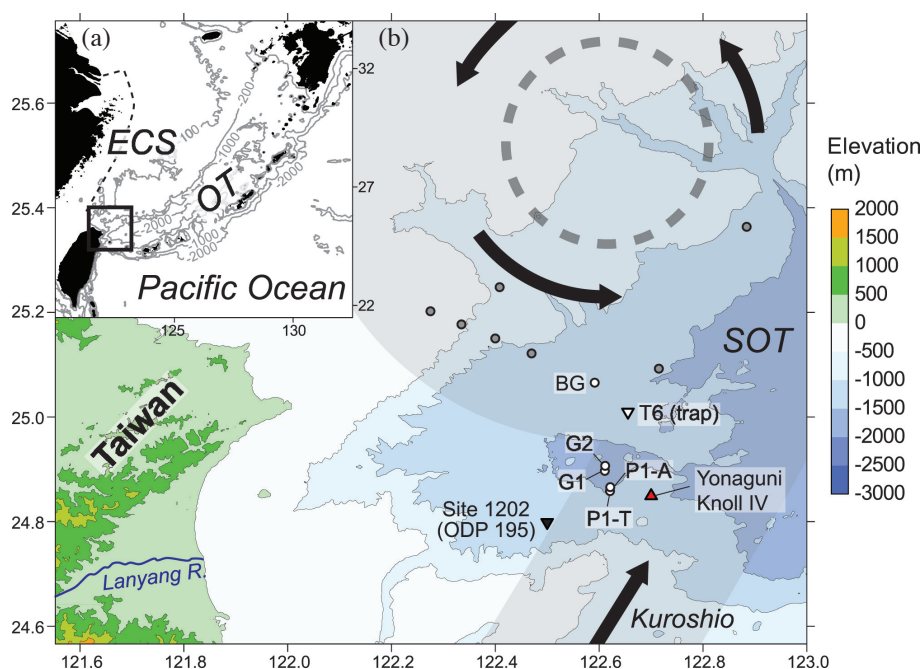


Fig. 1. (a) The location of the Okinawa Trough (OT) relative to the nearby landmasses and the East China Sea (ECS). The dash line stands for the inner shelf region defined in Kao et al. (2003). The square in bold line marks the region enlarged in (b). (b) The Southern Okinawa Trough (SOT) and sampling sites. Site T6 is a sediment trap station reported in previous studies (Sheu et al. 1999; Hsu et al. 2003). Gray dots denote the sites reported in Lin et al. (2002a). The gray shade and arrows indicate the route of the Kuroshio Current and its intrusion onto the East China Sea shelf. The dash circle designates the upwelling center induced by the cyclonic eddy. ODP, Ocean Drilling Program.

Table 1. Coordinates, water depth, and bulk solid-phase properties of the sites

Site	Cast type ^a	Longitude (E)	Latitude (N)	Water depth (m)	Porosity	TOC ^b (%wt)	TS (%wt)	Fe _T (%wt)	Mn _T (μg g ⁻¹)	
									0 - 1 cm	> 1 cm
BG	CTD, MUC	122°35.432'	25°03.075'	1387	-	-	-	-	-	-
P1-A	MUC	122°36.764'	24°50.921'	1512	0.65 - 0.73	0.72 ± 0.07 ^c	0.10 ± 0.01	4.33 ± 0.27	1230	529 ± 32
P1-T	CTD, MUC	122°37.222'	24°50.752'	1490	0.60 - 0.83	0.74 ± 0.10	0.10 ± 0.01	4.46 ± 0.18	2503	579 ± 149
P1-T	GC	122°37.204'	24°50.683'	1490	0.57 - 0.83	0.70 ± 0.23	0.15 ± 0.04	4.37 ± 0.30	584	504 ± 25
G1	CTD	122°36.580'	24°53.050'	1518	-	-	-	-	-	-
G2	MUC	122°36.598'	24°53.385'	1516	0.72 - 0.84	0.58 ± 0.06	0.10 ± 0.01	4.37 ± 0.30	1003	522 ± 53

Note: a: CTD, conductivity, temperature and depth instrument; GC, gravity core; MUC, multicore. b: Abbreviations: TOC, total organic carbon; TS, total sulfur; Fe_T, total iron; Mn_T, total manganese. c: The bulk properties of the solid phase were reported as the mean and standard error of measurements at depth resolutions of 5 - 20 cm.

and P1-T was carried out using a dissolved oxygen sensor (SBE 43, Sea-Bird Scientific), mounted on a conductivity, temperature, and depth (CTD) instrument. Sediment O₂ microprofiling was performed only at Site BG, visited during OR1-1194. Multicores were kept at 4°C without stirring for 8 h before analysis. We used Clark-type microelectrodes (OX-100, Unisense) with an outside tip diameter of 100 μm. The microelectrodes were two-point calibrated with air-saturated seawater and anoxic sediment pore waters at 3 - 5 cm depth.

2.4 Analysis

Nutrients (NO₃⁻ and NH₄⁺) were analyzed colorimetrically with a gas-segmented continuous flow auto-analyzer (QuAatro, SEAL Analytical Inc.). A certified reference material (MOOS-3, provided by the National Research Council, Canada) and in-house seawater nutrient standards (from Merck, traceable to NIST SRMs) were used to check the accuracy and precision. The analytical precision was 1.8% for NO₃⁻ and 5.5% for NH₄⁺.

For determination of Fe and Mn, fluid samples were analyzed on an inductively coupled plasma optical emission spectrometer (Optima 8000, Perkin-Elmer). High-purity standard solutions (High-Purity Standards, Inc.) of multi-elements were used to prepare a series of calibration solutions for Fe and Mn measurements. The analytical precision is 6.4 and 5.8% for Fe and Mn, respectively, for overlying water samples, and 4.8 and 1.8% for pore-water samples.

SO₄²⁻ was analyzed on an ion chromatography system (DIONEX ICS-3000, Thermo), and calibrated with standard solutions prepared from Merck Anionen-Mehrelement standard II. The precision was better than 2%. H₂S was measured by the methylene blue method (American Public Health Association, American Water Works Association and Water Environment Federation 1998) with a precision of ~5%. CH₄ was measured with a precision of ~3% using a gas chromatograph equipped with a flame ionization detector (Model 8610C, SRI Instruments). Detailed setup and discussion of the accuracy, precision and detection limits of this system were described in Lee (2004). Bottom-water DIC was measured by a dissolved inorganic analyzer (Model AS-C3; Apollo SciTech Inc.). Standard seawater (certified reference material prepared by the Scripps Institution of Oceanography) was used to check the accuracy and precision (0.1%). Pore-water DIC was determined using a Shimadzu TOC-Vcph carbon analyzer (Shimadzu Corp.). Repeated analyses of an in-house standard yielded a precision of 2%.

Porosity was determined following the procedure described in Blum (1997), assuming a pore-water density of 1.027 g cm⁻³. For determination of TOC content, dried sediment was decalcified and analyzed with an elemental analyzer (Flash 2000, Thermo Fisher Scientific). Repeated analyses of a certified soil standard (certificate number 133317, Thermo Fisher Scientific) yielded a precision of 3%. Desalted sediment samples were shipped to the Bureau Veritas Mineral Laboratories for the determination of TS, Fe_T, and Mn_T. The accuracy was assessed with the reference material OREAS 25a (Ore Research & Exploration Pty. Ltd.).

2.5 Calculation

With the assumption that the pore-water profiles were at a steady state, we used the software PROFILE (Berg et al. 1998) to calculate the net production rates of dissolved species. This software accounts for depth-dependent porosity profiles and resolves specific depth horizons in which net production or consumption takes place. The resulting rate values were depth-integrated (R , in mmol m⁻² d⁻¹) and converted to rates of organic carbon remineralization (C_{diag} , in mmol C m⁻² d⁻¹) assuming Redfield composition of sedimentary organic matter (e.g., Helder 1989; Bakker and Helder 1993):

$$C_{\text{diag}} = \alpha R \quad (1)$$

where α is a conversion factor derived from the stoichiometry of organic matter oxidation by different electron acceptors (Table 2; Aller 2014).

The burial rate of organic carbon (C_{burial}) across a sediment horizon at the depth of z ($z = 30$ cm for the discussion below) was calculated by the following equation (Lin et al. 2000):

$$C_{\text{burial}} = \rho(1 - \varphi)\omega[\text{TOC}]_z \quad (2)$$

where ρ is the dry bulk density (2.65 g cm⁻³), ω the sedimentation rate (0.4 cm yr⁻¹ for our sites; C. C. Su, unpublished data), and $[\text{TOC}]_z$ the TOC content at the depth z . The sum of C_{diag} and C_{burial} , defined as C_{proc} , represents the flux of organic carbon that reaches the seafloor and is processed thereunder (cf. Reimers and Suess 1983, for a detailed definition of different carbon fractions used in the literature of early diagenesis).

3. RESULTS

3.1 Solid-Phase Properties

The solid-phase properties of the sediment samples are listed in Table 1. The porosity varied within the range of 0.57 - 0.84. The TOC contents were in the range of 0.6 - 0.7%, statistically indistinguishable from previously reported contents of TOC in the SOT sediment (p-value = 0.07 - 0.28; Welch's t-test, two-tailed; Kao et al. 2003). The TS contents were on average 0.10% in the multicorer sediment, and slightly higher (~0.15%) in the deeper sediment of the gravity core (Table 1). The TS contents were consistent with the sum of pyrite and acid volatile sulfide contents presented in Lin et al. (2002a; p-value = 0.07 - 0.11). The Fe_T contents were about 4.4%. The Mn_T contents of the top 1 cm sediment (1000 - 2500 μg g⁻¹) were 2 - 5 folds higher than those of deeper sediments (~500 μg g⁻¹). The Fe_T and Mn_T contents were generally comparable to those reported for deep sediment trap samples and surface sediments (p-value = 0.56 - 0.81; Hsu et al. 2003).

3.2 O₂ Profiles

Dissolved O₂ exhibited a similar pattern in the water column at Sites BG, G1, and P1-T, with the concentration decreasing from ~200 μmol L⁻¹ in the surface water to 66 - 69 μmol L⁻¹ in the bottom water (Fig. 2a). The O₂ concentrations of overlying water were ~6 μmol L⁻¹ higher than the deep-water values obtained by the CTD casts (Fig. 2b). O₂ penetrated down to 1 cm below the seafloor. The curve was sigmoidal, caused by a top layer (0 - 0.08 cm) with enhanced advective transport (advection) overlying deeper layers dominated by diffusive transport (Bakker and Helder 1993).

The mismatch in O₂ concentration between the deep

Table 2. Overall stoichiometric organic matter oxidation reactions discussed in the present study. The coefficients in bold fonts are used in the conversion factor [α of Eq. (1)].

Redox process	Overall reaction
Aerobic respiration	$(\text{CH}_2\text{O})_{106}(\text{NH}_3)_{16}(\text{H}_3\text{PO}_4) + 138 \text{ O}_2 \rightarrow 106 \text{ CO}_2 + 122 \text{ H}_2\text{O} + 16 \text{ HNO}_3 + \text{H}_3\text{PO}_4$
Nitrate reduction	$(\text{CH}_2\text{O})_{106}(\text{NH}_3)_{16}(\text{H}_3\text{PO}_4) + 84.8 \text{ NO}_3^- \rightarrow 21.2 \text{ CO}_2 + 63.6 \text{ H}_2\text{O} + 84.8 \text{ HCO}_3^- + 42.4 \text{ N}_2 + 16 \text{ NH}_3 + \text{H}_3\text{PO}_4$
Manganese reduction	$(\text{CH}_2\text{O})_{106}(\text{NH}_3)_{16}(\text{H}_3\text{PO}_4) + 212 \text{ MnO}_2 + 318 \text{ CO}_2 + 106 \text{ H}_2\text{O} \rightarrow 212 \text{ Mn}^{2+} + 424 \text{ HCO}_3^- + 16 \text{ NH}_3 + \text{H}_3\text{PO}_4$
Iron reduction	$(\text{CH}_2\text{O})_{106}(\text{NH}_3)_{16}(\text{H}_3\text{PO}_4) + 424 \text{ Fe}(\text{OH})_3 + 742 \text{ CO}_2 \rightarrow 424 \text{ Fe}^{2+} + 848 \text{ HCO}_3^- + 318 \text{ H}_2\text{O} + 16 \text{ NH}_3 + \text{H}_3\text{PO}_4$
Sulfate reduction	$(\text{CH}_2\text{O})_{106}(\text{NH}_3)_{16}(\text{H}_3\text{PO}_4) + 53 \text{ SO}_4^{2-} \rightarrow 53 \text{ H}_2\text{S} + 106 \text{ HCO}_3^- + 16 \text{ NH}_3 + \text{H}_3\text{PO}_4$

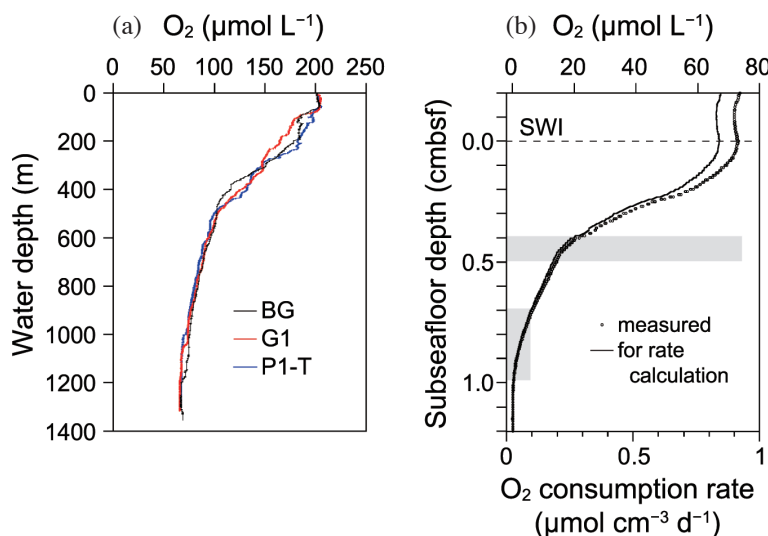


Fig. 2. (a) Distribution of O_2 in the water column at three stations. (b) Measured O_2 profile at Site BG and the adjusted profile for rate calculation. The gray shades denote the net O_2 consumption rate (gray shades) in different horizons. SWI, sediment-water interface.

seawater and overlying water has been observed before and attributed to exposure of cores to air during processing on deck (Helder 1989). Using the software PROFILE, we obtained two zones with net O_2 consumption (Fig. 2b). The rates are $0.93 \mu\text{mol cm}^{-3} \text{ d}^{-1}$ at 0.4 - 0.5 cm and $0.09 \mu\text{mol cm}^{-3} \text{ d}^{-1}$ at 0.7 - 1.0 cm. Following previous work (e.g., Hyun et al. 2017), we attributed the upper zone to O_2 consumption by aerobic organotrophic respiration, and the deeper zone to reoxidation of reduced substances.

3.3 Pore-Water Profiles

NO_3^- concentration in the topmost pore-water samples (Fig. 3) was $10 - 20 \mu\text{mol L}^{-1}$ lower than the deep seawater NO_3^- content ($36 \mu\text{mol L}^{-1}$; Wong et al. 1989), indicating active denitrification in the topmost 1 cm layer. NO_3^- concentration decreased exponentially with depth and was no longer detectable below 15 - 20 cm. A subsurface maximum was found at 15 and 13 cm in the profile of Site P1-T and G2, respectively. This feature has been found in other deep-sea sediments (e.g., Bakker and Helder 1993; Hyun et al. 2017) and is attributed to bioirrigating burrows. NH_4^+ ex-

hibited a downcore increasing trend, rising from a submicromolar level in the bottom water to $100 - 380 \mu\text{mol L}^{-1}$ at the bottom of the multicores.

Dissolved Mn concentration was $< 1 \mu\text{mol L}^{-1}$ in the deep seawater. In the interstitial space, Mn (presumably in the form of Mn^{2+}) accumulated rapidly, reaching $45 - 65 \mu\text{mol L}^{-1}$ in the top 5 - 6 cm. Below this top accumulation zone, Mn^{2+} concentrations decreased by $\sim 20 \mu\text{mol L}^{-1}$ and then continued to increase with depth. In the long gravity core of Site P1-T, the maximum Mn^{2+} concentration was reached at 55 cm, below which a decreasing trend with depth ensued. Dissolved Fe concentration was below the detection limit in the deep seawater. In the multicores, dissolved Fe (presumably in the form of Fe^{2+}) concentration increased with depth and reached $185 - 450 \mu\text{mol L}^{-1}$ at the core bottom. In the gravity core of Site P1-T, Fe^{2+} concentration showed a maximum at a depth of 60 cm and decreased with depth to $\sim 90 \mu\text{mol L}^{-1}$ at 115 cm.

Like the profiles of deep-water stations reported in Lin et al. (2002a), SO_4^{2-} concentrations were relatively constant, deviating less than 2 mmol L^{-1} from the bottom-water concentration throughout the cored sediment. H_2S concentrations

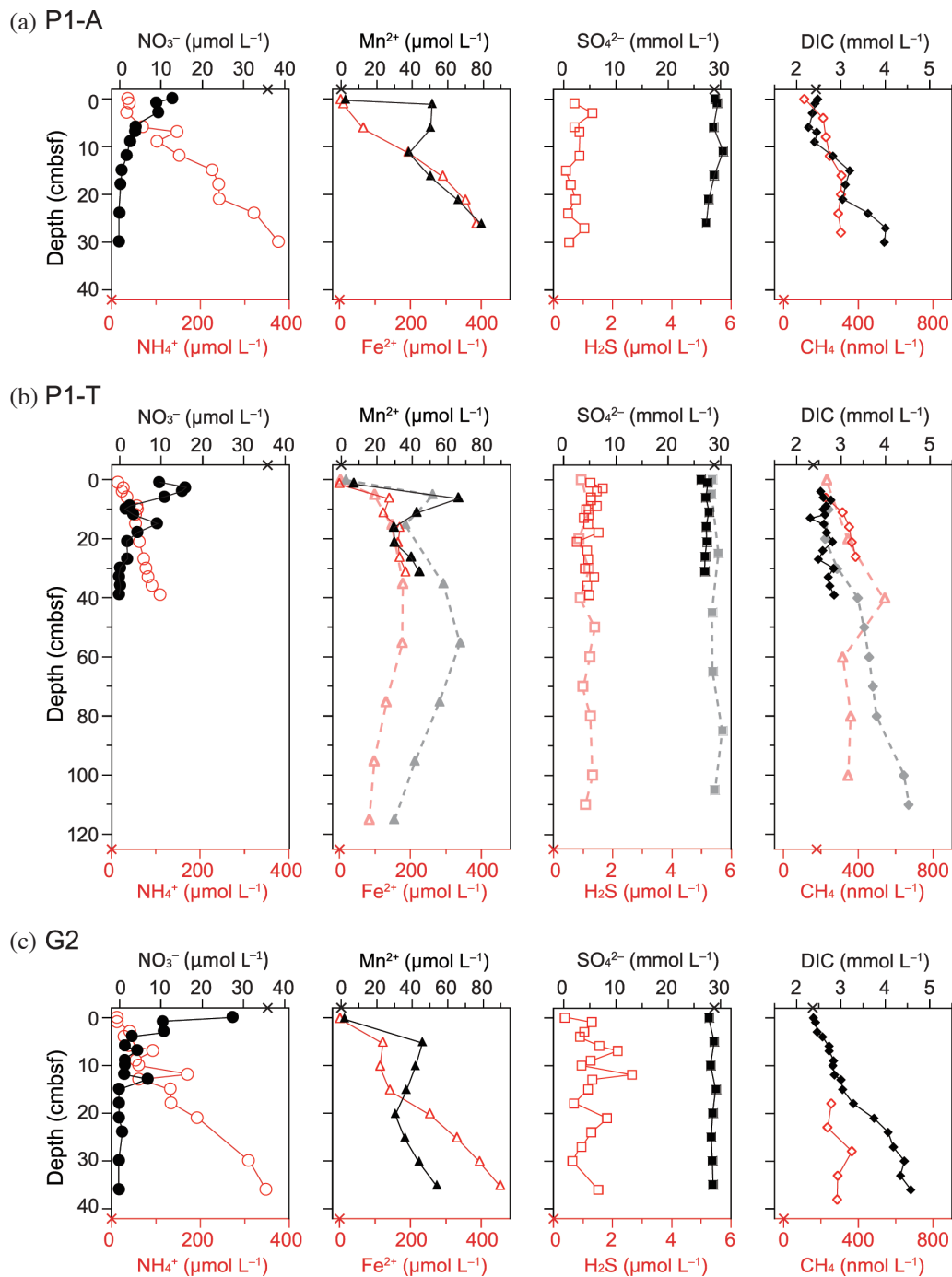


Fig. 3. Results of pore-water analyses at Sites (a) P1-A, (b) P1-T, and (c) G2. Gray and light red symbols with dash line denote data from the gravity core. Crosses on the x axes denote the solute concentration in the bottom water.

were constantly low but detectable ($0.4 - 2.7 \mu\text{mol L}^{-1}$). Some of the measurements might have been affected by the colored (slightly yellowish) substance in the pore water. The colored substance may be iron hydroxide precipitates, but we did not perform any correction on the photometric data.

At Sites P1-A and G2, DIC exhibited a downcore increasing trend, rising from deep seawater concentrations of $\sim 2.4 \text{ mmol L}^{-1}$ to $4 - 4.5 \text{ mmol L}^{-1}$ at the bottom of the multicore. Site P1-T showed a much gentler trend of DIC, reaching only 2.8 mmol L^{-1} at the bottom of the multicore and 4.5 mmol L^{-1} at the bottom of the gravity core. Pore-water CH_4 concentrations were in the range of $110 - 425 \text{ nmol L}^{-1}$ and exhibited a downcore increasing trend in the multicores. The concentration range is orders of magnitude lower than the typical range known for methanogenic sediment (millimolar scale; e.g., Lin et al. 2012). Of note is that dissolved CH_4 concentrations in the deep water of SOT are up to $100 - 500 \text{ nmol L}^{-1}$ (Hsu et al. 2003). Therefore, a portion of the pore-water CH_4 might have originated from the entrained bottom water during particle deposition.

Using the software PROFILE, we computed the depth-integrated production rates of NO_3^- , Mn^{2+} , Fe^{2+} and NH_4^+ (Table 3). The consumption rates of NO_3^- ($234 - 436 \mu\text{mol m}^{-2} \text{ d}^{-1}$) are higher than the production rates of dissolved metals ($24 - 160 \mu\text{mol m}^{-2} \text{ d}^{-1}$). The production rates of NH_4^+ exhibited inter-site variations, ranging from $23 - 76 \mu\text{mol m}^{-2} \text{ d}^{-1}$.

4. DISCUSSION

Although the initial purpose of the sampling campaign was to investigate the geochemistry of sediments altered by hydrothermal activities, the bulk properties of our sediment, such as TOC, TS, Fe_T and Mn_T (Table 1), are all statistically indistinguishable from the values reported previously for regular SOT sediment. Moreover, in spite of the elevated values of $^3\text{He}/^4\text{He}$ ratios (T. Lan, unpublished data), the pore-water profiles did not exhibit signatures known for liquid CO_2 -impregnated sediments, such as exceptionally high total alkalinity or DIC at the tens of millimolar level, and

the rapid decrease of SO_4^{2-} within the upper 30 cm (De Beer et al. 2013). Liquid CO_2 impregnation and the associated geochemical characteristics are the main features of hydrothermally altered sediment in this backarc basin (Inagaki et al. 2006; De Beer et al. 2013). Therefore, we conclude that our sites are only marginally affected by hydrothermal activities, and the pore-water profiles reflect the general diagenetic condition in the deep SOT.

Pore-water profiles are sensitive to the quantity and quality of remineralizable carbon, the supply of which is governed by regional oceanographic and depositional environments. Based on bulk properties and molecular proxies, several studies support the notion that a major fraction of organic matter in SOT sediment originates from the inner shelf of ECS (Kao et al. 2003; Chen et al. 2017). The shelf-exported organic matter that ultimately reaches the deep SOT might be extensively processed, but the regional upwelling center (Fig. 1) may add degradable carbon to the seafloor. To clarify the effects of these factors on the observed diagenetic activity, in the following discussion, we compare our data primarily with those of ECS sediment. Where appropriate, other systems at comparable water depths are also discussed.

4.1 Early Diagenetic Features of SOT Sediments

The pore-water profiles in the short multicores (Figs. 2 and 3) have the following key features for dissolved species related to terminal electron accepting processes. O_2 was exhausted a depth of 1 cm with a change in the concentration gradient at 0.45 cm, associated with a zone of active O_2 consumption. NO_3^- consumption occurred even with the presence of O_2 in the top 1 cm, and NO_3^- exhaustion depths occurred at ~ 15 cm. Mn and Fe reduction occurred within 1 - 5 cm where NO_3^- concentrations remain abundant ($10 - 15 \mu\text{mol L}^{-1}$). Mn and Fe profiles are highly smeared, increased to a maximum but decreased again with depths (Fig. 3). The downward decreasing trend in deeper sediment is interpreted as the solubility control of authigenic phases, such as Mn carbonates and Fe sulfides (Canfield et

Table 3. Depth-integrated net production rates (R , in $\text{mmol m}^{-2} \text{ d}^{-1}$) of dissolved species in the upper 30 cm sediment. Negative rate values represent net consumption. Depth range (in cm) is the range of reaction zones identified by the software PROFILE (Berg et al. 1998).

Species	BG		P1-A		P1-T		G2	
	Depth range	R						
O_2	0.40 - 0.50	-1.20	-	-	-	-	-	-
NO_3^-	-	-	0 - 2	-0.44	0 - 2	-0.28	0 - 2	-0.23
Mn^{2+}	-	-	0 - 2	0.16	5 - 7	0.03	0 - 7	0.02 ^a
Fe^{2+}	-	-	0 - 16	0.03	3 - 7	0.08	0 - 6	0.13
NH_4^+	-	-	10 - 25	0.05	10 - 12	0.02	25 - 30	0.08

Note: a: Rates underestimated due to a lower sampling resolution.

al. 1993). The zigzag feature of Mn^{2+} profiles is not uncommon in marine sediment (e.g., Canfield et al. 1993), but the underlying reason is barely discussed. This is possibly due to the fact that both Mn^{2+} and MnO_2 can couple to multiple redox species other than organic matter (Aller 2014), complicating the interpretation of Mn data as a manifestation of a carbon oxidation process. Sulfate reduction is not significant because SO_4^{2-} concentrations are relatively unchanged, and the methanogenic zone is below the examined interval (125 cm). The observation is consistent with the data of ODP Site 1202 (from Ocean Drilling Program Leg 195), drilled 11 km southeast to our sites (Fig. 1). The long core showed that the sulfate-methane interface is as deep as 10 m (Mottl 2005).

4.2 Comparison of Pore-Water Profiles of SOT and ECS Sediments

The features summarized above differ in several aspects from those reported for ECS sediments. Most of the pore-water geochemical studies of ECS are based on sediments retrieved in the inner shelf (Fig. 1) during summer. The water depths of ECS are shallow (10 - 63 m) and thus the bottom water is characterized with high O_2 concentrations (100 - 220 $\mu\text{mol L}^{-1}$; Chen et al. 2007) and low NO_3^- concentrations (mostly < 10 $\mu\text{mol L}^{-1}$; Gong et al. 2000) except the estuaries, where anthropogenic input is significant. Nevertheless, the O_2 penetration depth is as shallow as 0.3 - 0.7 cm in the reported sediment profiles, giving rise to steep concentration gradients (Cai et al. 2014). NO_3^- profiles are highly heterogeneous for the shelf sites. Some showed an extended NO_3^- -rich upper layer up to 10 cm in thickness, others showed a rapid decrease in the top 5 cm, and still others had subsurface NO_3^- maximums (Song et al. 2013; Zhao et al. 2017). Observable gradients of $\text{SO}_4^{2-}/\text{Cl}^-$ ratio were found in about half of the published profiles (Zhao et al. 2017). The gentler O_2 gradients, deeper O_2 penetration and a lack of marked SO_4^{2-} concentration gradients indicate lower diagenetic activity in SOT sediments than in inner shelf sediments of ECS.

Like SOT sediment, most of the Mn^{2+} profiles of ECS showed a steep gradient in the top 1 cm and reached maximum levels of 30 - 80 $\mu\text{mol L}^{-1}$ (Zhao et al. 2017). However, a downcore decreasing trend of Mn^{2+} below the subsurface maximum could be readily observed in the 30 cm sediment column, alluding to a higher flux of substances for precipitating Mn^{2+} out of the aqueous phase in ECS sediments than in SOT sediments. A change in curvature could also be seen in the Fe^{2+} profiles, with subsurface maximum mostly < 100 $\mu\text{mol L}^{-1}$ (Zhao et al. 2017).

Interpretation of the differences in Mn^{2+} and Fe^{2+} profiles from SOT and ECS is less straightforward, as the abundance of these solutes also depends on the supply of reactive metal species in the solid phase and co-precipitation agents

(e.g., CO_3^{2-} and S^{2-}) in the pore fluids. The extremely high Fe^{2+} concentrations (up to 450 $\mu\text{mol L}^{-1}$) and the smeared Fe^{2+} profiles in SOT sediments are distinct from Fe^{2+} in other continental slope sediments at comparable water depths, where Fe^{2+} contents barely exceed 50 $\mu\text{mol L}^{-1}$ (e.g., Helder 1989; Küster-Heins et al. 2010; Hyun et al. 2017). The Mn_T and Fe_T contents in the surface sediment of our cored sites are comparable to those in the inner shelf sediments of the ECS (Lin et al. 2002b; Zhu et al. 2012). However, at the species level, Hsu et al. (2003) reported enrichment of reactive Mn and Fe in the settling particles of the sediment trap station T6 (Fig. 1) because of incorporation of hydrothermally derived particles. In their 1340-m trap samples, the sum of exchangeable, carbonate, and easily-to-moderately reducible Mn and Fe fractions constitutes 86 ± 6 and $41 \pm 1\%$, respectively, of the Mn_T and Fe_T . If the deep-water trap samples are good approximations of surface sediment samples in terms of solid-phase composition, surface sediments of SOT would be enriched in reactive Fe relative to those of ECS ($33 \pm 4\%$; Zhu et al. 2012). Therefore, the pore-water Fe^{2+} features of SOT is attributed to (1) the addition of hydrothermally-derived Fe, which provides for the iron reducing communities, and (2) the sluggish sulfate reduction (Lin et al. 2002a), which supplies H_2S slowly for removing dissolved Fe from soluble phase.

By corollary, one would anticipate the same smeared shape and high concentrations for the Mn^{2+} profiles. The SOT sediments do have smeared Mn^{2+} profiles relative to ECS sediments, but the maximum concentrations are not significantly elevated. This could be either due to leakage of Mn^{2+} from the sediment into overlying water (Hyun et al. 2017), strong adsorption of Mn^{2+} onto Mn oxides (Canfield et al. 1993), or other as yet unaccounted-for processes. The impact of hydrothermally derived Mn precipitates on diagenesis, if present, remains elusive and awaits clarification via incubation-based approaches.

4.3 Partitioning of Carbon Oxidation Pathways

One classical approach of quantifying diagenetic activities is to convert production or consumption rates of redox-related dissolved species into rates of organic carbon remineralization by the use of Redfield stoichiometry [Eq. (1)]. This approach, though not as accurate as tracer techniques (Reimers and Suess 1983), provides an initial quantitative assessment of diagenetic activities. As pore-water analysis is more frequently carried out than tracer experiments, this approach furnishes a common basis for comparison across different systems.

We calculated the C_{diag} rates (Table 4) by different electron acceptors using the depth-integrated net production or consumption rates of dissolved species (Table 3). Although sedimentary O_2 data are not available at Sites P1-A, P1-T, and G2, the O_2 consumption rate of Site BG is only slightly

lower than that determined for regular sediment in the nearby Yonaguni Knoll IV ($1.51 \text{ mmol O}_2 \text{ m}^{-2} \text{ d}^{-1}$; calculated from De Beer et al. 2013). It is possible that the actual O_2 consumption rates of the other three sites fall around the values determined for Site BG and Yonaguni Knoll IV, and minor deviations in O_2 consumption rates from the Site BG value would not change our conclusions. The SO_4^{2-} gradient is barely detectable except for Site P1-A, which showed a decrease in SO_4^{2-} by 2 mmol L^{-1} at the core bottom. The production of NH_4^+ , instead, exceeds the theoretical contribution by Fe reduction (cf. Table 2 for the stoichiometry). Therefore, we used the excess NH_4^+ production rate, i.e., the rate that cannot be accounted for by Fe reduction, to estimate of the amount of carbon oxidized by sulfate reduction. The resulting C_{diag} rates of $0.30 \pm 0.17 \text{ mmol C m}^{-2} \text{ d}^{-1}$ agree within uncertainties with the radioactive tracer-based estimate ($0.34 \text{ mmol C m}^{-2} \text{ d}^{-1}$ for the deep-water station; calculated from Lin et al. 2002a). The

total C_{diag} rates for the upper 30 cm sediment column are $1.68 \pm 0.21 \text{ mmol C m}^{-2} \text{ d}^{-1}$. The total C_{diag} rates are low, being only $\sim 70\%$ of the values of the Savu Basin sediments in Indonesia ($2.42 \pm 0.51 \text{ mmol C m}^{-2} \text{ d}^{-1}$; $\sim 2000 \text{ m}$ water depth; Helder 1989) or the aerobic carbon oxidation rates of East Sea sediments in Northeast Asia ($2.52 \pm 1.65 \text{ mmol C m}^{-2} \text{ d}^{-1}$; $1500 - 2000 \text{ m}$ water depth; Hyun et al. 2017). The contribution of different electron acceptors, in decreasing order of relative importance, is O_2 ($55 \pm 7\%$) $>$ NO_3^- ($24 \pm 8\%$) \approx SO_4^{2-} ($18 \pm 10\%$) $>$ Mn oxides ($2 \pm 2\%$) \approx Fe oxides ($1.2 \pm 0.8\%$).

A similar practice was performed using literature data of inner shelf sediments in the ECS (Table 5). We are aware that due to seasonal variations in weather and current conditions, the pore-water profiles are not under a steady state at an annual time scale. Therefore, we based our calculation only on data of one single season, and the results should not be extrapolated to annual estimates. We obtained a total

Table 4. Areal rates of carbon oxidation via early diagenesis (C_{diag}), derived from the depth-integrated net production rates of dissolved species listed in Table 3, for the upper 30 cm sediment.

Carbon remineralization by:	Conversion factor (α) ^a	C_{diag} (mmol C m ⁻² d ⁻¹)				Average over sites			
		BG	P1-A	P1-T	G2	C_{diag} (mmol C m ⁻² d ⁻¹)		Relative importance (%)	
						Mean	σ	Mean	σ
Aerobic respiration	106/138	0.92	-	-	-	0.92	-	55	7
NO_3^- reduction	106/84.8	-	0.54	0.35	0.29	0.40	0.13	24	8
Mn reduction	106/212	-	0.08	0.02	0.01 ^b	0.04	0.04	2	2
Fe reduction	106/424	-	0.007	0.02	0.03	0.02	0.01	1.2	0.8
SO_4^{2-} reduction	106/16	-	0.31	0.14	0.47	0.30	0.17	18	10
Total	-	-	-	-	-	1.68	0.21	100	

Note: a: Conversion factor is the stoichiometric ratio used to calculate carbon remineralization rates from net production or consumption rates of dissolved species based on stoichiometric organic matter oxidation reactions (Table 2). The carbon remineralization rates by SO_4^{2-} reduction was calculated from the production rates of excess NH_4^+ , i.e., rates that cannot be accounted for by Fe reduction. b: Rates underestimated due to a lower sampling resolution.

Table 5. Depth-integrated net production rates (R) of dissolved species, the corresponding C_{diag} rates, and the relative importance of each process in diagenetic carbon oxidation in East China Sea sediments. Integration depth: 30 cm.

Carbon remineralization by:	R (mmol m ⁻² d ⁻¹)	C_{diag} rate (mmol C m ⁻² d ⁻¹)	Relative importance (%)	Method	Reference
Aerobic respiration	15.90 ± 2.39 (1.2-25.6) ^a	12.21 ± 1.84	63 ± 15	O_2 microelectrodes	Cai et al. 2014
NO_3^- reduction	1.34 ± 1.09 (0.30-3.06)	1.68 ± 1.36	9 ± 7	Pore-water profiles analyzed by PROFILE ^b	Song et al. 2013
Mn oxides reduction	0.20 ± 0.19 (0.04-0.63)	0.10 ± 0.09	0.5 ± 0.5	Pore-water profiles analyzed by PROFILE	Zhao et al. 2017
Fe oxides reduction	0.15 ± 0.11 (0.03-0.44)	0.04 ± 0.03	0.2 ± 0.2	Pore-water profiles analyzed by PROFILE	Zhao et al. 2017
SO_4^{2-} reduction	2.72 ± 1.42 (1.7-6.0)	5.45 ± 2.83	28 ± 15	³⁵ S, whole core incubation	Lin et al. 2000
Total	20.31 ± 2.99	19.48 ± 3.62	100		

Note: a: Numbers in the parentheses indicate minimum and maximum values. b: The denitrification and dissimilatory nitrate reduction rates determined by ¹⁵N tracer experiments (Song et al. 2013) are not included in the calculation due to the high concentration ($100 \mu\text{mol L}^{-1}$) of ¹⁵ NO_3^- applied in the incubation.

C_{diag} rate of $19.48 \pm 3.62 \text{ mmol C m}^{-2} \text{ d}^{-1}$ for the ECS sediment in summer (Table 5), with the relative importance of different electron acceptors decreasing in the order of O_2 ($63 \pm 15\%$) > SO_4^{2-} ($28 \pm 15\%$) > NO_3^- ($9 \pm 7\%$) > Mn oxides ($0.5 \pm 0.5\%$) \approx Fe oxides ($0.2 \pm 0.2\%$).

Comparison of the C_{diag} data of SOT and ECS revealed several intriguing features. First, while the SOT sediments have TOC contents (0.4 - 0.7%; Kao et al. 2003) only slightly lower than those of ECS inner shelf sediments (0.4 - 1.0%; Zhu et al. 2012), C_{diag} rates of the former are one order of magnitude lower than the latter. Second, despite the distinct bottom-water O_2 concentrations of the inner shelf (the cited O_2 profiles of ECS sediment were not generated in the hypoxia region) and in the trough, aerobic respiration is the dominant redox process in both systems. Lastly, the relative importance of nitrate reduction in organic carbon oxidation is elevated in SOT compared with ECS sediments. Associations of these features to the quantity and quality of organic carbon, bottom-water conditions, and methodological limitations will be elaborated in succeeding text.

4.4 Budget, Quality and Burial Efficiency of Organic Carbon

To assess the quantity and quality of organic carbon, we first evaluated the benthic-pelagic carbon budget for the SOT and ECS regions (Fig. 4). The SOT has a clear component of vertical transport. The primary production at the trap station T6 is $24 \pm 1 \text{ mmol C m}^{-2} \text{ d}^{-1}$ (Gong et al. 2000). Based on the sediment trap data (Sheu et al. 1999), lateral transport is present but mild under regular conditions (i.e., not during episodic flood events). The C_{proc} (cf. section 2.5)

is $5.2 \pm 2.3 \text{ mmol C m}^{-2} \text{ d}^{-1}$, in agreement with the flux measured at 1346 m of Station T6.

Such a budget has already been presented previously for the ECS (Song et al. 2016). Here, we slightly modified the existing ECS budget by using our own estimates of C_{diag} (Table 5) to cover the diagenetic activity of 30 cm sediment column. The C_{proc} for the ECS is $26.3 \pm 8.0 \text{ mmol C m}^{-2} \text{ d}^{-1}$, much lower than the trap-derived settling fluxes (200 - 300 $\text{mmol C m}^{-2} \text{ d}^{-1}$ in the inner shelf; Zhang et al. 2006) or the primary production ($78 \pm 53 \text{ mmol C m}^{-2} \text{ d}^{-1}$; Gong et al. 2003). The unbalanced budget reflects the steering role of lateral transport and resuspension, both of which are difficult to quantify, in governing the deposition and distribution of organic carbon on the shelf.

Because C_{proc} is less sensitive to resuspension compared with sediment trap measurements, the quality of organic carbon is assessed by the ratio $C_{\text{diag}}/C_{\text{proc}}$. To take into account that C_{diag} rates, like all microbial activities, are temperature dependent (Price and Sowers 2004), we first calculated the theoretical C_{diag} value at 4°C ($C_{\text{diag},4^\circ\text{C}}$) assuming a temperature coefficient (Q_{10}) of 2:

$$C_{\text{diag},4^\circ\text{C}} = C_{\text{diag}} Q_{10}^{(4^\circ\text{C} - T_{\text{in situ}})/10^\circ} \quad (3)$$

The in situ bottom-water temperature ($T_{\text{in situ}}$) in summer is 20°C for the ECS (Song et al. 2016). The $C_{\text{diag},4^\circ\text{C}}$ value of ECS ($6.4 \pm 1.2 \text{ mmol C m}^{-2} \text{ d}^{-1}$) remains significantly higher than that of SOT, but the $C_{\text{diag},4^\circ\text{C}}/C_{\text{proc}}$ ratios (ECS, 0.24 ± 0.09 ; SOT, 0.32 ± 0.15) no longer indicate a higher proportion of degradable organic carbon on the shelf. Accordingly, there is no conclusive evidence for a lower quality of organic

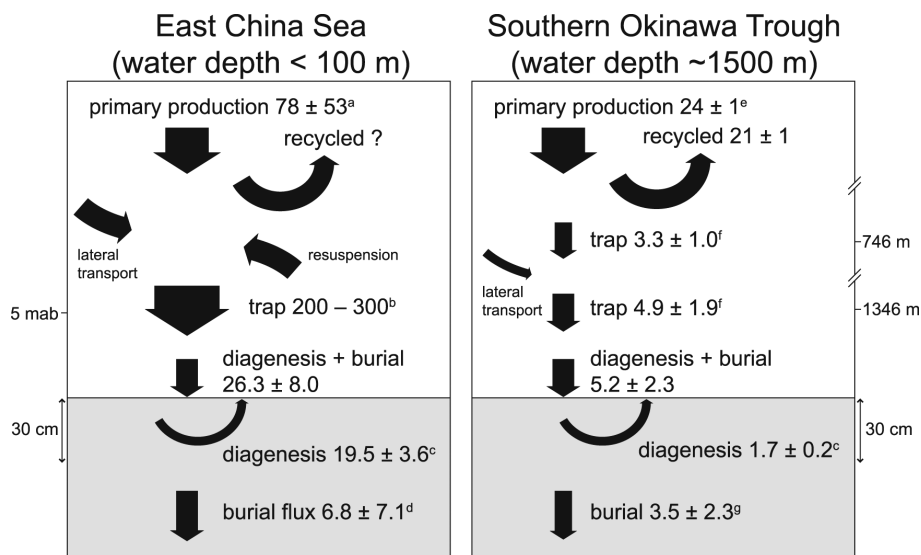


Fig. 4. A simple pelagic-benthic budget for organic carbon flux in the ECS and deep SOT. The fluxes are in the unit of $\text{mmol m}^{-2} \text{ d}^{-1}$. Sources: a = Gong et al. (2003); b = Zhang et al. (2006); c = this study; d = Song et al. (2016); e = Gong et al. (2000); f = Sheu et al. (1999); g = Lin et al. (2002a) and this study. Abbreviation: mab, meters above bottom.

matter in the SOT. This finding seems to contradict the presumption that the SOT, being the terminal of cross-shelf sediment transport (Kao et al. 2003; Chen et al. 2017) and vertical deposition, should receive particles containing relatively refractory organic matter. Uncertainties in the estimates of C_{diag} , the use of an inappropriate Q_{10} value, or the presence of unaccounted sources of labile carbon (e.g., fresh phytodetritus from the perennial upwelling center; Fig. 1) might result in the lack of a significant difference in the $C_{\text{diag}, 4^{\circ}\text{C}}/C_{\text{proc}}$ ratios between the two systems. Further degradation experiments are necessary to clarify this issue. Based on the existing data, we tentatively attribute the 10-fold difference in C_{diag} rate to different bottom-water temperature and carbon flux.

The burial efficiency, assessed by $C_{\text{burial}}/C_{\text{proc}} \times 100\%$, is 68 and 26% for the SOT and ECS, respectively. With net sediment accumulation rates available for both regions (Su and Huh 2002; Li et al. 2012), their carbon preservation efficiency can be further compared with other major depositional systems around the world (Fig. 5; Blair and Aller 2012). The SOT plots next to continental boundaries fed by small mountain rivers, whereas the inner shelf of ECS dots the region defined for deltaic fluidized muds.

The proximity of the inner shelf sediments of ECS to deltaic fluidized muds in Fig. 5 alludes to the same controlling mechanism of the low carbon burial efficiency, i.e., prolonged exposure of particles to oxygen-rich water as a result of frequent sediment reworking and suspension (Blair and Aller 2012). The controlling mechanisms of the high carbon burial efficiency in the SOT are more complicated,

including the factors of small mountain rivers and rifting. These two factors act differently in facilitating carbon burial. Small mountain rivers actively deliver deposits containing fossil organic carbon during storm events (Blair and Aller 2012), whereas rifting works passively via creating steep topographic gradients and deep basins. The steep gradients induce geofocusing of particles toward the bottom, whereas the deep water depth results in prolonged alteration of phytodetritus during vertical transport and suppressed microbial activities due to lowered bottom-water temperature (Price and Sowers 2004). The notion supported by previous studies, i.e., a major fraction of organic matter in SOT sediment originates from the inner shelf of ECS instead of rivers in northeastern Taiwan (Kao et al. 2003; Chen et al. 2017), argues in favor of a greater contribution from rifting over small mountain rivers. However, mineralogical evidence suggests that rivers in northeastern Taiwan (Fig. 1) provide massive clastic materials to the SOT (Diekmann et al. 2008), implying substantial contribution of fossil organic carbon to the high burial efficiency. To clarify whether and how rifting alone can elevate carbon sequestration, further study is warranted to investigate the early diagenesis of regular sediment in the central section of the Okinawa Trough, which is distant from major mountain rivers in Taiwan and Japan.

4.5 Effects of Bottom-Water Conditions and Methodological Limitations

The deep basin of SOT is a suboxic environment

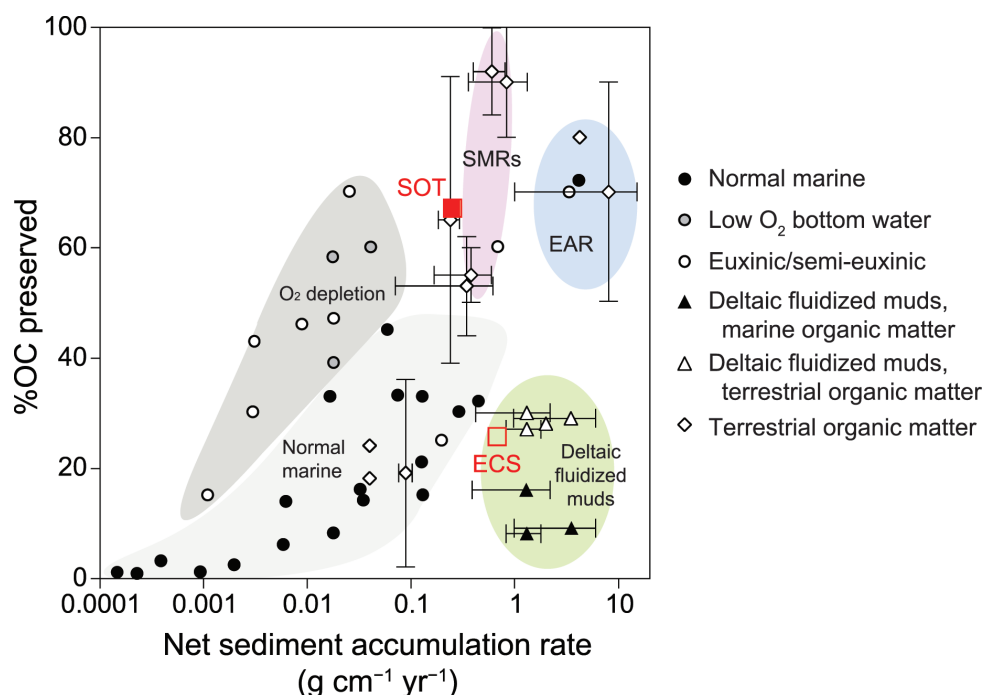


Fig. 5. The percentage of organic carbon (OC) preserved versus net sediment accumulation rate of the SOT, ECS (inner shelf), and major depositional environments (modified from Blair and Aller 2012). Abbreviations: EAR, extreme accumulation rates; SMRs, small mountain rivers.

with low O_2 (66 - 69 $\mu\text{mol L}^{-1}$; Fig. 2a) and high NO_3^- (36 $\mu\text{mol L}^{-1}$; Wong et al. 1989) concentrations. This bottom-water condition is in contrast to that of the ECS, which is relatively enriched in O_2 (mostly > 100 $\mu\text{mol L}^{-1}$ except for the hypoxia region; Chen et al. 2007) and depleted in NO_3^- (mostly < 10 $\mu\text{mol L}^{-1}$; Gong et al. 2000). Hence, our findings of reduced contribution of O_2 and elevated contribution of NO_3^- in the SOT, compared to those of the ECS, likely reflect the control of bottom-water conditions on the partitioning of carbon oxidation processes in near-surface sediment, as suggested by earlier modelling work (e.g., Soetaert et al. 1996).

Lastly, it is necessary to acknowledge the limitations of this pore-water profile-based approach in quantifying early diagenesis. First, it is not common to have the complete suite of redox-related dissolved species characterized in one single site. For example, the pore-water data from the ECS are collected from different sites. Given the high heterogeneity of shelf water and sediment, the composite partitioning scheme of carbon oxidation pathways might have errors larger than presented in Table 5. Second, it is well-known that dissolved Mn^{2+} and Fe^{2+} profiles generally lead to underestimation of Mn and Fe oxides reduction (Canfield et al. 1993; Hyun et al. 2017). This is because Mn^{2+} and Fe^{2+} also accumulate in the solid phase, which represents the major fraction of the reduced pools. For example, the rates of Fe reduction calculated by the pore-water profiles of the East Sea sediments are two to three orders of magnitudes lower than those obtained via incubations (Hyun et al. 2017), and Fe reduction contributes up to 20% of carbon oxidation. Lastly, this approach does not consider the aerobic carbon remineralization contributed by faunal activities (i.e., $C_{\text{pre-burial}}$ in Reimers and Suess 1983), including bioturbation, bioirrigation and metabolic demands (Glud 2008; Snelgrove et al. 2018). Therefore, the partitioning of carbon oxidation pathways summarized in this study for the SOT and ECS sediments (Table 5) should be considered tentative. Additional studies using incubation-based techniques are sorely needed to revise the partitioning scheme, and to better estimate the C_{diag} rate.

5. CONCLUSION

This study presents an examination of diagenetic activities and carbon remineralization based on the first complete suite of pore-water data of sediment marginally affected by hydrothermal activities in the SOT. Below is a summary of our main findings.

(1) The pore-water data show an oxygen penetration depth of 1 cm, consumption of NO_3^- in the top 1 cm, smeared profiles of Mn^{2+} and Fe^{2+} with the latter reaching up to 450 $\mu\text{mol L}^{-1}$, and relatively unchanged SO_4^{2-} concentrations with depth. The remarkably high Fe^{2+} concentrations possibly reflect the incorporation of hydrothermal-

ly derived reactive Fe into settling particles.

- (2) Analysis of the pore-water profiles provides an estimate of $1.68 \pm 0.21 \text{ mmol C m}^{-2} \text{ d}^{-1}$ as the total carbon remineralization rate in the upper 30 cm sediment column. The rate, about 10-fold lower than that of ECS, is attributed to the lower bottom-water temperature and carbon flux in the trough.
- (3) Compared to the ECS, the relative importance of O_2 and NO_3^- as electron acceptors is reduced and enhanced, respectively, in the SOT, reflecting the control of bottom-water conditions on early diagenesis. However, aerobic respiration remains the major carbon oxidation pathway.
- (4) The SOT has a carbon burial efficiency of 68%, and plots close to continental boundaries fed by small mountain rivers on the carbon preservation-mass accumulation graph. The high carbon burial efficiency reflects the combined effects of small mountain rivers and rifting-induced particle geofocusing and refrigerating.

Acknowledgements We thank the captains and crews of the R/V *Ocean Researcher I* for their competent work. We are grateful to Bing-Rong Jiang, Shu-Han Chang, Sheng-Ting Hsu, and Yi-Jyun Chen for their assistance on sampling and lab work, and Ai-Lin Lyu for logistic support. We thank the two anonymous reviewers for their constructive comments. This work was financed by the Central Geologic Survey, Ministry of Economic Affairs.

REFERENCES

- Aller, R. C., 2014: Sedimentary diagenesis, depositional environments, and benthic fluxes. In: Holland, H. D. and K. K. Turekian (Eds.), *Treatise on Geochemistry*, Second Edition, Vol. 8, Elsevier, Amsterdam, 293-334, doi: 10.1016/B978-0-08-095975-7.00611-2. [[Link](#)]
- American Public Health Association, American Water Works Association and Water Environment Federation, 1998: *Standard Methods for the Examination of Water and Wastewater*, Method 4500-S $_2^-$ sulfide, American Public Health Association, Washington, D.C., USA, 1220 pp.
- Bakker, J. F. and W. Helder, 1993: Skagerrak (northeastern North Sea) oxygen microprofiles and porewater chemistry in sediments. *Mar. Geol.*, **111**, 299-321, doi: 10.1016/0025-3227(93)90137-K. [[Link](#)]
- Berg, P., N. Risgaard-Petersen, and S. Rysgaard, 1998: Interpretation of measured concentration profiles in sediment pore water. *Limnol. Oceanogr.*, **43**, 1500-1510, doi: 10.4319/lo.1998.43.7.1500. [[Link](#)]
- Berndt, C., C. Hensen, C. Mortera-Gutierrez, S. Sarkar, S. Geilert, M. Schmidt, V. Liebetrau, R. Kipfer, F. Scholz, M. Doll, S. Muff, J. Karstens, S. Planke, S. Petersen, C. Böttner, W.-C. Chi, M. Moser, R. Behrendt, A. Fiskal, M. A. Lever, C. C. Su, L. Deng, M.

- S. Brennwald, and D. Lizarralde, 2016: Rifting under steam—How rift magmatism triggers methane venting from sedimentary basins. *Geology*, **44**, 767-770, doi: 10.1130/G38049.1. [[Link](#)]
- Blair, N. E. and R. C. Aller, 2012: The fate of terrestrial organic carbon in the marine environment. *Annu. Rev. Mar. Sci.*, **4**, 401-423, doi: 10.1146/annurev-marine-120709-142717. [[Link](#)]
- Blum, P., 1997: Physical properties handbook: A guide to the shipboard measurement of physical properties of deep-sea cores. ODP Technical Note 26, doi: 10.2973/odp.tn.26.1997. [[Link](#)]
- Boudreau, B. P., 1987: A steady-state diagenetic model for dissolved carbonate species and pH in the porewaters of oxic and suboxic sediments. *Geochim. Cosmochim. Acta*, **51**, 1985-1996, doi: 10.1016/0016-7037(87)90187-6. [[Link](#)]
- Cai, P., X. Shi, W. S. Moore, S. Peng, G. Wang, and M. Dai, 2014: ^{224}Ra : ^{228}Th disequilibrium in coastal sediments: Implications for solute transfer across the sediment-water interface. *Geochim. Cosmochim. Acta*, **125**, 68-84, doi: 10.1016/j.gca.2013.09.029. [[Link](#)]
- Calvert, S. E., 1966: Accumulation of diatomaceous silica in the sediments of the Gulf of California. *Geol. Soc. Am. Bull.*, **77**, 569-596, doi: 10.1130/0016-7606(1966)77[569:AODSIT]2.0.CO;2. [[Link](#)]
- Canfield, D. E., B. Thamdrup, and J. W. Hansen, 1993: The anaerobic degradation of organic matter in Danish coastal sediments: Iron reduction, manganese reduction, and sulfate reduction. *Geochim. Cosmochim. Acta*, **57**, 3867-3883, doi: 10.1016/0016-7037(93)90340-3. [[Link](#)]
- Chen, C. C., G. C. Gong, and F. K. Shiah, 2007: Hypoxia in the East China Sea: One of the largest coastal low-oxygen areas in the world. *Mar. Environ. Res.*, **64**, 399-408, doi: 10.1016/j.marenvres.2007.01.007. [[Link](#)]
- Chen, C.-T. A., S. Kandasamy, Y. P. Chang, Y. Bai, X. He, J. T. Lu, and X. Gao, 2017: Geochemical evidence of the indirect pathway of terrestrial particulate material transport to the Okinawa Trough. *Quat. Int.*, **441**, 51-61, doi: 10.1016/j.quaint.2016.08.006. [[Link](#)]
- Chou, Y.-C., C.-C. Wang, H.-H. Chen, and Y.-H. Lin, 2019: Seafloor characterization in the southernmost Okinawa Trough from underwater optical imagery. *Terr. Atmos. Ocean. Sci.*, **30**, 717-737, doi: 10.3319/TAO.2019.03.14.01. [[Link](#)]
- De Beer, D., M. Haeckel, J. Neumann, G. Wegener, F. Inagaki, and A. Boetius, 2013: Saturated CO₂ inhibits microbial processes in CO₂-vented deep-sea sediments. *Biogeosciences*, **10**, 5639-5649, doi: 10.5194/bg-10-5639-2013. [[Link](#)]
- Diekmann, B., J. Hofmann, R. Henrich, D. K. Fütterer, U. Röhl, and K. Y. Wei, 2008: Detrital sediment supply in the southern Okinawa Trough and its relation to sea-level and Kuroshio dynamics during the late Quaternary. *Mar. Geol.*, **255**, 83-95, doi: 10.1016/j.margeo.2008.08.001. [[Link](#)]
- Emerson, S., R. Jahnke, M. Bender, P. Froelich, G. Klinkhammer, C. Bowser, and G. Setlock, 1980: Early diagenesis in sediments from the Eastern Equatorial Pacific, I. Pore water nutrient and carbonate results. *Earth Planet. Sci. Lett.*, **49**, 57-80, doi: 10.1016/0012-821X(80)90150-8. [[Link](#)]
- Glasby, G. P. and K. Notsu, 2003: Submarine hydrothermal mineralization in the Okinawa Trough, SW of Japan: An overview. *Ore Geol. Rev.*, **23**, 299-339, doi: 10.1016/j.oregeorev.2003.07.001. [[Link](#)]
- Glud, R. N., 2008: Oxygen dynamics of marine sediments. *Mar. Biol. Res.*, **4**, 243-289, doi: 10.1080/17451000801888726. [[Link](#)]
- Gong, G.-C., F.-K. Shiah, K.-K. Liu, Y.-H. Wen, and M.-H. Liang, 2000: Spatial and temporal variation of chlorophyll *a*, primary productivity and chemical hydrography in the southern East China Sea. *Cont. Shelf Res.*, **20**, 411-436, doi: 10.1016/S0278-4343(99)00079-5. [[Link](#)]
- Gong, G.-C., Y.-H. Wen, B.-W. Wang, and G.-J. Liu, 2003: Seasonal variation of chlorophyll *a* concentration, primary production and environmental conditions in the subtropical East China Sea. *Deep-Sea Res. Part II-Top. Stud. Oceanogr.*, **50**, 1219-1236, doi: 10.1016/S0967-0645(03)00019-5. [[Link](#)]
- Helder, W., 1989: Early diagenesis and sediment-water exchange in the Savu Basin (Eastern Indonesia). *Neth. J. Sea Res.*, **24**, 555-572, doi: 10.1016/0077-7579(89)90133-6. [[Link](#)]
- Hsu, H.-H., L.-F. Lin, C.-S. Liu, J.-H. Chang, W.-Z. Liao, T.-T. Chen, K.-H. Chao, S.-L. Lin, H.-S. Hsieh, and S.-C. Chen, 2019: Pseudo-3D seismic imaging of Geolin Mounds hydrothermal field in the Southern Okinawa Trough offshore NE Taiwan. *Terr. Atmos. Ocean. Sci.*, **30**, 705-716, doi: 10.3319/TAO.2019.03.14.02. [[Link](#)]
- Hsu, S. C., F. J. Lin, W. L. Jeng, Y. C. Chung, and L. M. Shaw, 2003: Hydrothermal signatures in the southern Okinawa Trough detected by the sequential extraction of settling particles. *Mar. Chem.*, **84**, 49-66, doi: 10.1016/S0304-4203(03)00102-6. [[Link](#)]
- Huh, C. A., C. C. Su, C. H. Wang, S. Y. Lee, and I. T. Lin, 2006: Sedimentation in the Southern Okinawa Trough—Rates, turbidites and a sediment budget. *Mar. Geol.*, **231**, 129-139, doi: 10.1016/j.margeo.2006.05.009. [[Link](#)]
- Hyun, J. H., S. H. Kim, J. S. Mok, H. Cho, T. Lee, V. Vandieken, and B. Thamdrup, 2017: Manganese and iron reduction dominate organic carbon oxidation in surface sediments of the deep Ulleung Basin, East Sea. *Biogeosciences*, **14**, 941-958, doi: 10.5194/bg-14-941-2017. [[Link](#)]

- Inagaki, F., M. M. M. Kuypers, U. Tsunogai, J. Ishibashi, K. Nakamura, T. Treude, S. Ohkubo, M. Nakaseama, K. Gena, H. Chiba, H. Hirayama, T. Nunoura, K. Takai, B. B. Jørgensen, K. Horikoshi, and A. Boetius, 2006: Microbial community in a sediment-hosted CO₂ lake of the southern Okinawa Trough hydrothermal system. *Proc. Natl. Acad. Sci.*, **103**, 14164-14169, doi: 10.1073/pnas.0606083103. [Link]
- Kao, S. J., F. J. Lin, and K. K. Liu, 2003: Organic carbon and nitrogen contents and their isotopic compositions in surficial sediments from the East China Sea shelf and the southern Okinawa Trough. *Deep-Sea Res. Part II-Top. Stud. Oceanogr.*, **50**, 1203-1217, doi: 10.1016/S0967-0645(03)00018-3. [Link]
- Konno, U., U. Tsunogai, F. Nakagawa, M. Nakaseama, J. Ishibashi, T. Nunoura, and K. Nakamura, 2006: Liquid CO₂ venting on the seafloor: Yonaguni Knoll IV hydrothermal system, Okinawa Trough. *Geophys. Res. Lett.*, **33**, L16607, doi: 10.1029/2006GL026115. [Link]
- Küster-Heins, K., G. J. de Lange, and M. Zabel, 2010: Benthic phosphorus and iron budgets for three NW African slope sediments: A balance approach. *Biogeosciences*, **7**, 469-480, doi: 10.5194/bg-7-469-2010. [Link]
- Lee, H. F., 2004: Compositions of Fumarolic Gases and the H-O Isotopic Ratios of the Condensed Water in Tatun Volcanic Area, North Taiwan. Master Thesis, Institute of Geoscience, National Taiwan University, Taipei City, Taiwan, 83 pp, doi: 10.6342/NTU.2004.02083. (in Chinese) [Link]
- Li, J., B. Hu, Y. Dou, J. Zhao, and G. Li, 2012: Modern sedimentation rate, budget and supply of the muddy deposits in the East China Seas. *Geological Review*, **58**, 745-756. (in Chinese)
- Lin, S., K. M. Huang, and S. K. Chen, 2000: Organic carbon deposition and its control on iron sulfide formation of the southern East China Sea continental shelf sediments. *Cont. Shelf Res.*, **20**, 619-635, doi: 10.1016/S0278-4343(99)00088-6. [Link]
- Lin, S., K. M. Huang, and S. K. Chen, 2002a: Sulfate reduction and iron sulfide mineral formation in the southern East China Sea continental slope sediment. *Deep-Sea Res. Part I-Oceanogr. Res. Pap.*, **49**, 1837-1852, doi: 10.1016/S0967-0637(02)00092-4. [Link]
- Lin, S., I. J. Hsieh, K. M. Huang, and C. H. Wang, 2002b: Influence of the Yangtze River and grain size on the spatial variations of heavy metals and organic carbon in the East China Sea continental shelf sediments. *Chem. Geol.*, **182**, 377-394, doi: 10.1016/S0009-2541(01)00331-X. [Link]
- Lin, Y. S., V. B. Heuer, T. Goldhammer, M. Y. Kellermann, M. Zabel, and K. U. Hinrichs, 2012: Towards constraining H₂ concentration in subseafloor sediment: A proposal for combined analysis by two distinct approaches. *Geochim. Cosmochim. Acta*, **77**, 186-201, doi: 10.1016/j.gca.2011.11.008. [Link]
- Lin, Y. S., B. P. Koch, T. Feseker, K. Ziervogel, T. Goldhammer, F. Schmidt, M. Witt, M. Y. Kellermann, M. Zabel, A. Teske, and K. U. Hinrichs, 2017: Near-surface heating of young rift sediment causes mass production and discharge of reactive dissolved organic matter. *Sci. Rep.*, **7**, doi: 10.1038/srep44864. [Link]
- Liu, K. K., G. C. Gong, S. Lin, C. Y. Yang, C. L. Wei, S. C. Pai, and C. K. Wu, 1992: The year-round upwelling at the shelf break near the northern tip of Taiwan as evidenced by chemical hydrography. *Terr. Atmos. Ocean. Sci.*, **3**, 243-276, doi: 10.3319/TAO.1992.3.3.243(KEEP). [Link]
- Lizarralde, D., S. A. Soule, J. S. Seewald, and G. Proskurowski, 2011: Carbon release by off-axis magmatism in a young sedimented spreading centre. *Nat. Geosci.*, **4**, 50-54, doi: 10.1038/ngeo1006. [Link]
- Mottl, M. J., 2005: Data report: Composition of pore water from Site 1202, southern Okinawa Trough. In: Shinohara, M., M. H. Salisbury, and C. Richter (Eds.), Proceedings of the Ocean Drilling Program, Scientific Results, 195. Available at http://www-odp.tamu.edu/publications/195_SR/107/107.htm.
- Price, P. B. and T. Sowers, 2004: Temperature dependence of metabolic rates for microbial growth, maintenance, and survival. *Proc. Natl. Acad. Sci.*, **101**, 4631-4636, doi: 10.1073/pnas.0400522101. [Link]
- Reimers, C. E. and E. Suess, 1983: The partitioning of organic carbon fluxes and sedimentary organic matter decomposition rates in the ocean. *Mar. Chem.*, **13**, 141-168, doi: 10.1016/0304-4203(83)90022-1. [Link]
- Sakai, H., T. Gamo, E. Kim, K. Shitashima, F. Yanagisawa, M. Tsutsumi, J. Ishibashi, Y. Sano, H. Wakita, T. Tanaka, T. Matsumoto, T. Naganuma, and K. Mitsuzawa, 1990: Unique chemistry of the hydrothermal solution in the Mid-Okinawa Trough backarc basin. *Geophys. Res. Lett.*, **17**, 2133-2136, doi: 10.1029/GL017i012p02133. [Link]
- Seeberg-Elverfeldt, J., M. Schlüter, T. Feseker, and M. Kölling, 2005: Rhizon sampling of porewaters near the sediment-water interface of aquatic systems. *Limnol. Oceanogr. Meth.*, **3**, 361-371, doi: 10.4319/lom.2005.3.361. [Link]
- Sheu, D. D., W. C. Jou, Y. C. Chung, T. Y. Tang, and J. J. Hung, 1999: Geochemical and carbon isotopic characterization of particles collected in sediment traps from the East China Sea continental slope and the Okinawa Trough northeast of Taiwan. *Cont. Shelf Res.*, **19**, 183-203, doi: 10.1016/S0278-4343(98)00081-8. [Link]
- Sibuet, J. C., B. Deffontaines, S. K. Hsu, N. Thureau, J. P. Le Formal, and C. S. Liu, 1998: Okinawa trough backarc basin: Early tectonic and magmatic evolution. *J. Geophys. Res.*, **103**, 30245-30267, doi: 10.1029/98JB01823. [Link]

- Snelgrove, P. V. R., K. Soetaert, M. Solan, S. Thrush, C.-L. Wei, R. Danovaro, R. W. Fulweiler, H. Kitazato, B. Ingole, A. Norkko, R. J. Parkes, and N. Volkenborn, 2018: Global carbon cycling on a heterogeneous seafloor. *Trends Ecol. Evol.*, **33**, 96-105, doi: 10.1016/j.tree.2017.11.004. [[Link](#)]
- Soetaert, K., P. M. Herman, and J. J. Middelburg, 1996: A model of early diagenetic processes from the shelf to abyssal depths. *Geochim. Cosmochim. Acta*, **60**, 1019-1040, doi: 10.1016/0016-7037(96)00013-0. [[Link](#)]
- Song, G. D., S. M. Liu, H. Marchant, M. M. M. Kuypers, and G. Lavik, 2013: Anammox, denitrification and dissimilatory nitrate reduction to ammonium in the East China Sea sediment. *Biogeosciences*, **10**, 6851-6864, doi: 10.5194/bg-10-6851-2013. [[Link](#)]
- Song, G. D., S. Liu, Z. Zhu, W. Zhai, C. Zhu, and J. Zhang, 2016: Sediment oxygen consumption and benthic organic carbon mineralization on the continental shelves of the East China Sea and the Yellow Sea. *Deep-Sea Res. Part II-Top. Stud. Oceanogr.*, **124**, 53-63, doi: 10.1016/j.dsr2.2015.04.012. [[Link](#)]
- Su, C.-C. and C.-A. Huh, 2002: ^{210}Pb , ^{137}Cs and $^{239,240}\text{Pu}$ in East China Sea sediments: Sources, pathways and budgets of sediments and radionuclides. *Mar. Geol.*, **183**, 163-178, doi: 10.1016/s0025-3227(02)00165-2. [[Link](#)]
- Thunell, R. C., C. J. Pride, E. Tappa, and F. E. Muller-Karger, 1994: Biogenic silica fluxes and accumulation rates in the Gulf of California. *Geology*, **22**, 303-306, doi: 10.1130/0091-7613(1994)022<0303:BSFAAR>2.3.CO;2. [[Link](#)]
- Wong, G. T. F., S. C. Pai, and C. T. A. Chen, 1989: Chemical hydrography across the East China Sea - Kuroshio frontal region, northeast of Taiwan. *Acta Oceanogr. Taiwan*, **23**, 1-18.
- Zhang, Y., F. Zhang, X. Guo, and M. Zhang, 2006: Autumn flux of particle settling observed at three representative stations in East China Sea. *Oceanologia et Limnologia Sinica*, **37**, 28-34. (in Chinese)
- Zhao, B., P. Yao, T. S. Bianchi, Y. Xu, H. Liu, T. Mi, X. H. Zhang, J. Liu, and Z. Yu, 2017: Early diagenesis and authigenic mineral formation in mobile muds of the Changjiang Estuary and adjacent shelf. *J. Mar. Syst.*, **172**, 64-74, doi: 10.1016/j.jmarsys.2017.03.001. [[Link](#)]
- Zhu, M. X., X. C. Hao, X. N. Shi, G. P. Yang, and T. Li, 2012: Speciation and spatial distribution of solid-phase iron in surface sediments of the East China Sea continental shelf. *Appl. Geochem.*, **27**, 892-905, doi: 10.1016/j.apgeochem.2012.01.004. [[Link](#)]